Upgraded VIRGO detector(s) and stochastic gravitational waves backgrounds

D. Babusci[(a)] * and M. Giovannini[(b)]†
[(a)] *INFN - Laboratori Nazionali di Frascati, 00044 Frascati, Italy*
[(b)] *Institute for Theoretical Physics, Lausanne University, BSP-Dorigny, CH-1015 Switzerland*

The sensitivity achievable by a pair of VIRGO detectors to stochastic and isotropic gravitational wave backgrounds of cosmological origin is discussed in view of the development of a second VIRGO interferometer. We describe a semi-analytical technique allowing to compute the signal-to-noise ratio for (monotonic or non-monotonic) logarithmic energy spectra of relic gravitons of arbitrary slope. We apply our results to the case of two correlated and coaligned VIRGO detectors and we compute their achievable sensitivities. The maximization of the overlap reduction function is discussed. We focus our attention on a class of models whose expected sensitivity is more promising, namely the case of string cosmological gravitons. We perform our calculations both for the case of minimal string cosmological scenario and in the case of a non-minimal scenario where a long dilaton dominated phase is present prior to the onset of the ordinary radiation dominated phase. In this framework, we study possible improvements of the achievable sensitivities by selective reduction of the thermal contributions (pendulum and pendulum's internal modes) to the noise power spectra of the detectors. Since a reduction of the shot noise does not increase significantly the expected sensitivity of a VIRGO pair (in spite of the relative spatial location of the two detectors) our findings support the experimental efforts directed towards a substantial reduction of thermal noise.

I. THE PROBLEM AND ITS MOTIVATIONS

It is well known that every variation of the background geometry produces graviton pairs which are stochastically distributed and whose logarithmic energy spectra represent a faithful snapshot of the (time) evolution of the curvature scale at very early times [1]. Indeed, one of the peculiar features of stochastic graviton backgrounds is that their energy spectra extend over a huge interval of (present) frequencies. This feature can be appreciated by comparing the graviton backgrounds with other backgrounds of electromagnetic origin (like the cosmic microwave background [CMB]). The analysis of the CMB background (together with its spatial anisotropies) is relevant for very large (length) scales [2] (roughly ranging between the present horizon [i.e. 10^{-18} Hz] and the horizon at decoupling [i.e. 10^{-16} Hz]). Since gravitational interactions are much weaker than electromagnetic interactions they also decouple much earlier and, therefore, the logarithmic energy spectra of relic gravitons produced by the pumping action of the gravitational field can very well extend for (approximately) twenty five orders of magnitude in frequency [3]. From the physical point of view, this observation implies that the energy spectra of relic gravitons can be extremely relevant in order to probe the past history of the Universe in a regime which will never be directly accessible with observations of electromagnetic backgrounds.

In spite of the fact that the *nature* of the production mechanism is shared by different types of models [1], the specific *amplitudes of the energy spectra* can very well change depending upon the behavior of the background evolution. An example in this direction are logarithmic energy spectra increasing in frequency [4]. Different theoretical signals (with different spectral distributions) lead to detector outputs of different amplitudes. We are facing a non-linear problem where a change in the detector signal can be determined either by an improvement in the features of the detector or by a different functional form of the logarithmic energy spectrum [5]. Therefore, in order to evaluate the performances of a given detector one has to choose the specific functional form of the logarithmic energy spectrum. A possible choice is represented by scale invariant spectra [6,7]. Another rather interesting choice is represented by tilted ("blue" [8]) spectra whose energetical content is typically concentrated at frequencies larger than the mHz [9]. String cosmological models [10] are yet another interesting theoretical laboratory leading usually to sizable theoretical signals in the operating window of wide band interferometers (WBI) [11]. A possible detection of these backgrounds would represent an interesting test for cosmological models inspired by the low energy string effective action.

Every measurement in cosmology turns out to be difficult for different and independent reasons. The CMB anisotropy experiments have to cope with the mandatory subtraction of different electromagnetic foregrounds which

*Electronic address: danilo.babusci@lnf.infn.it
†Electronic address: Massimo.Giovannini@ipt.unil.ch

can be much larger than the "cosmological" signal one ought to detect. In order to detect gravitational waves of cosmological origin with terrestrial measurements we are facing similar problems.

The signal induced in the detector output by stochastic gravitational waves backgrounds is indistinguishable from the intrinsic noise of the detector itself. This implies that, unless the amplitude of the signal is very large, the only chance of direct detection of these backgrounds lies in the analysis of the correlated fluctuactions of the outputs of, at least, two detectors affected by independent noises. The problem of the optimal processing of the detector outputs required for the detection of the stochastic background has been considered by various authors [12,13] and it was also reviewed in ref. [14].

Suppose, indeed, that the signal registered at each detector can be written as (we limit ourselves to the case of two detectors ($i = 1, 2$))

$$s_i \, = \, h_i(t) \, + \, n_i(t) \, , \tag{1.1}$$

where we have indicated with n the intrinsic noise of the detector, and with h the gravitational strain due to the stochastic background. By assuming that the detector noises are stationary and uncorrelated, the ensemble average of their Fourier components satisfies

$$\langle n_i^*(f) \, n_j(f') \rangle \, = \, \frac{1}{2} \, \delta(f - f') \, \delta_{ij} \, S_n^{(i)}(|f|) \, , \tag{1.2}$$

where $S_n(|f|)$ is usually known as the one-sided noise power spectrum and is expressed in seconds. Starting to the signals s_1 and s_2, a correlation "signal" for an observation time T can be defined in the following way:

$$S \, = \, \int_{-T/2}^{T/2} \mathrm{d}t \, \int_{-T/2}^{T/2} \mathrm{d}t' \, s_1(t) \, s_2(t') \, Q(t - t') \tag{1.3}$$

where Q is a filter function that depends only by $t - t'$ because we assume that n and h are both stationary. The optimal choice of Q corresponds to the maximization of the signal-to-noise ratio associated to the "signal" S. Under the further assumptions that detector noises are Gaussian, much larger in amplitude than the gravitational strain and statistically independent on the strain itself, it can be shown [12–14] that the signal-to-noise ratio in a frequency range $(f_{\mathrm{m}}, f_{\mathrm{M}})$ is given by [1]:

$$\mathrm{SNR}^2 \, = \, \frac{3 H_0^2}{2\sqrt{2}\, \pi^2} \, F \, \sqrt{T} \, \left\{ \int_{f_{\mathrm{m}}}^{f_{\mathrm{M}}} \mathrm{d}f \, \frac{\gamma^2(f) \, \Omega_{\mathrm{GW}}^2(f)}{f^6 \, S_n^{(1)}(f) \, S_n^{(2)}(f)} \right\}^{1/2} \, , \tag{1.4}$$

where H_0 is the present value of the Hubble parameter and F is a numerical factor depending upon the geometry of the two detectors. In the case of the correlation between two interferometers $F = 2/5$, however, in the correlation of detectors of different geometry, $F \neq 2/5$ (see Appendix A for details about this point). In Eq. (1.4), the performances achievable by the pair of detectors are certainly controlled by the noise power spectra (NPS) $S_n^{(1,2)}$. However in Eq. (1.4), on top of NPS, there are two important quantities. The first one is the *theoretical* background signal defined through the logarithmic energy spectrum (normalized to the critical density ρ_c) and expressed at the present (conformal) time[2] η_0

$$\Omega_{\mathrm{GW}}(f, \eta_0) \, = \, \frac{1}{\rho_c} \, \frac{\mathrm{d}\rho_{\mathrm{GW}}}{\mathrm{d} \ln f} \, = \, \overline{\Omega}(\eta_0) \, \omega(f, \eta_0) \, . \tag{1.5}$$

The second one is the overlap reduction function $\gamma(f)$ [13,14] which is a dimensionless function describing the reduction in the sensitivity of the two detectors (at a given frequency f) arising from the fact that the two detectors are not in the same place and, in general, not coaligned (for the same location and orientation $\gamma(f) = 1$). Since the overlap reduction function cuts-off the integrand of Eq. (1.4) at a frequency which approximately corresponds to the inverse separation between the two detectors, it may represent a dangerous (but controllable) element in the reduction of the sensitivity of a given pair of detectors.

---

[1] In order to avoid possible confusions we stress that the definition of the SNR is the one discussed in [5] and it is essentially the square root of the one discussed in [12–14].

[2] In most of our equations we drop the dependence of spectral quantities upon the present time since all the quantities introduced in this paper are evaluated today.

Various ground-based interferometric detectors are presently under construction (GEO [15], LIGO-LA, LIGO-WA [16], TAMA [17], VIRGO [18]). Among them, the pair consisting of most homogeneous (from the point of view of the noise performances) detectors with minimum separation is given by the two LIGOs (VIRGO and GEO are even closer, but they have different performances for what concerns the NPS). However, this separation ($\simeq$ 3000 km) is still too large. The overlap reduction function $\gamma(f)$ for the pair LIGO-LA−LIGO-WA encounters its first zero at 64 Hz, falling off (swiftly) at higher frequencies, i.e., right in the region where the two LIGOs, at least in their initial version, have better noise performances.

Recently, within the european gravitational wave community, the possibility of building in Europe an interferometric detector of dimensions comparable to VIRGO has received close attention [19]. Therefore, there is a chance that in the near future the VIRGO detector, now under construction at Cascina (Pisa) in Italy, will be complemented by another interferometer of even better performances very close (at a distance $d < 1000$ km) to it. In this paper we examine in detail the possible improvements in the VIRGO sensitivity as a result of direct correlation of two VIRGO-like detectors. Furthermore, since technological improvements in the construction of the interferometers can be reasonably expected in the next years, it is easy to predict that also VIRGO, as for the LIGO detectors, will gradually evolve toward an advanced configuration. For this reason we also examine the possible consequences of a selective improvements of the noise characteristics of the two detectors on the obtained results.

In order to evaluate precisely the performances of a pair of VIRGO detectors we will use the following logic. First of all we will pick up a given class of theoretical models which look particularly promising in view of their spectral properties in the operating window of the WBI. Secondly we will analyze the signal-to-noise ratios for different regions of the parameter space of the model. Finally we will implement some selective reduction of the noises and we will compare the results with the ones obtained in the cases where the noises are not reduced. We will repeat the same procedure for different classes of models.

The results and the investigations we are reporting can be applied to spectra of arbitrary functional form. The only two requirements we assume will be the continuity of the logarithmic energy spectra (as a function of the present frequency) and of their first derivative. We will also give some other examples in this direction.

In order to make our analysis concrete we will pay particular attention to the evaluation of the performances of a pair of VIRGO detectors in the case of string cosmological models [10,11].

The plan of our paper is then the following. In Section II we introduce the basic semi-analytical tecnique which allows the evaluation of the SNR for a pair of WBI. In Section III we will evaluate the performances of a pair of VIRGO detectors in the case of string cosmological models. In Section IV we will show how to implement a selective noise reduction and we will investigate the impact of such a reduction in the case of the parameter space of the models previously analyzed. Section V contains our final discussion and the basic summary of our results. We collect in the Appendices some technical results useful for our analysis and other interesting complements to our investigation.

II. SNR EVALUATION

In the operating window of the VIRGO detectors the theoretical signal will be defined through the logarithmic energy spectrum reported in Eq. (1.5). In the present Section we shall not make any specific assumption concerning $\omega(f)$ and our results have general applicability. We will only assume that it is a continuous function of the frequency and we will also assume that its first derivative is well defined in the operating window of WBI. This means that $\omega(f)$ can be, in principle, a non-monotonic function.

A. Basic Formalism

The noise power spectrum of the VIRGO detector is well approximated by the analytical fit of Ref. [21], namely

$$\Sigma_n(f) \,=\, \frac{S_n(f)}{S_0} \,=\, \begin{cases} \infty & f < f_b \\ \Sigma_1 \left(\dfrac{f_{\rm a}}{f}\right)^5 \,+\, \Sigma_2 \left(\dfrac{f_{\rm a}}{f}\right) \,+\, \Sigma_3 \left[1 + \left(\dfrac{f}{f_{\rm a}}\right)^2\right], & f \geq f_b \end{cases} \tag{2.1}$$

where

$$S_0 \,=\, 10^{-44}\,{\rm s}\,, \qquad f_a \,=\, 500\,{\rm Hz}\,, \qquad f_b \,=\, 2\,{\rm Hz}\,, \qquad \begin{array}{l} \Sigma_1 \,=\, 3.46 \,\times\, 10^{-6} \\ \Sigma_2 \,=\, 6.60 \,\times\, 10^{-2} \\ \Sigma_3 \,=\, 3.24 \,\times\, 10^{-2}\,. \end{array}$$

In order to compute reliably (and beyond naive power counting arguments) the SNR we have to specify the overlap reduction function $\gamma(f)$. The relative location and orientation of the two detectors determines the functional form of $\gamma(f)$ which has to be gauged in such a way that the overlap between the two detectors is maximized (i.e. $\gamma(f) \simeq 1$ for most of the operating window of the two VIRGO). Moreover, the two interferometers of the pair should also be sufficiently far apart in order to decorrelate the local seismic and electromagnetic noises. Since the precise location of the second VIRGO detector has not been specified so far [19], we find useful to elaborate about this point by computing the overlap reduction functions corresponding to two coaligned VIRGO interferometers with different spatial separations. The results of these calculations are reported in Fig. 1. Needless to say that these choices are purely theoretical and are only meant to illustrate the effects of the distance on the performances of the VIRGO pair[3].

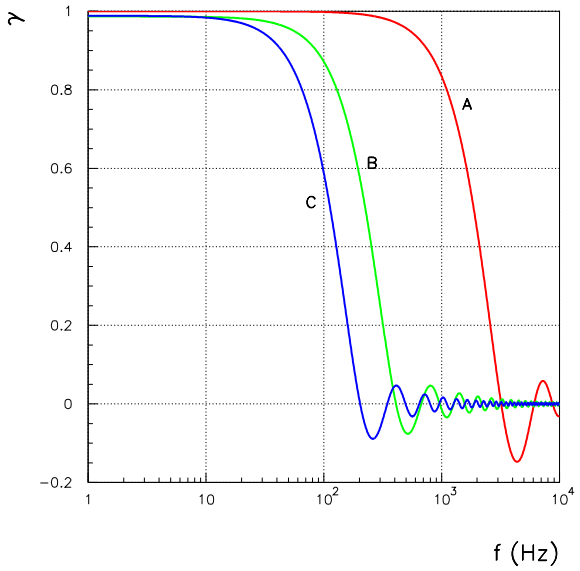

FIG. 1. We report the overlap reduction function(s) for the correlation of the VIRGO detector presently under construction in Cascina (43.6 N, 10.5 E) with a coaligned interferometer whose (corner) station is located at: A) (43.2 N, 10.9 E), $d = 58$ km (Italy); B) (43.6 N, 4.5 E), $d = 482.7$ km (France); C) (52.3 N, 9.8 E), $d = 958.2$ km (Germany). The third site (C) corresponds to the present location of the GEO detector. Notice that from A to C the position of the first zero of $\gamma(f)$ gets shifted in the infra-red. See also Appendix A concerning this last point.

The curves labeled with A, B, and C shown in Fig. 1 correspond to different distances d between the site of the VIRGO detector (presently under construction in Cascina, near Pisa) and the central corner station of a second coaligned VIRGO interferometer. Let us now look at the position of the first frequency f_i for which $\gamma(f_i) = 0$ for each of the curves. We can notice that by increasing d (i.e., going from A to C) the value of f_i gets progressively shifted towards lower and lower frequencies, linearly with d. This means that, for the specific purpose of the detection of a stochastic gravitational waves background, the position of the first zero of the overlap reduction function cannot be ignored. On a general ground we would like f_i to be slightly larger than the frequency region where the sensitivity of the pair of wide band detectors is maximal. In the explicit examples presented in this paper we will focus our attention on the case A. The other two configurations will be the subject of a related investigation [20].

[3]For illustrative purposes, we assumed that a distance of about 50 km is sufficient to decorrelate local seismic and e.m. noises. Such a hypothesis is fair at the present stage and it is certainly justified within the spirit of our exercise. However, at the moment, we do not have any indication either against or in favor of our choice.

B. SNR versus phenomenological bounds on the graviton spectrum

By inserting the parametrization (1.5) into Eq. (1.4) we can write

$$\mathrm{SNR}^2 \,=\, \frac{3H_0^2}{5\sqrt{2}\,\pi^2}\,\sqrt{T}\,\frac{\overline{\Omega}}{f_0^{5/2}\,S_0}\,J\,, \tag{2.2}$$

where we introduced the (dimension-less) integral

$$J^2 \,=\, \int_{\nu_{\rm m}}^{\nu_{\rm M}} {\rm d}\nu\,\frac{\gamma^2\,(f_0\nu)\,\omega^2(f_0\nu)}{\nu^6\,\Sigma_n^{(1)}(f_0\nu)\,\Sigma_n^{(2)}(f_0\nu)}\,. \tag{2.3}$$

Here the integration variable is $\nu \,=\, f/f_0$, with f_0 a generic frequency scale within the operating window of the interferometer, and the integration domain is restricted to the region $f_{\rm m} \,\leq\, f \,\leq\, f_{\rm M}$ (i.e., $\nu_{\rm m} \,\leq\, \nu \,\leq\, \nu_{\rm M}$). In the following we will choose $f_0 \,=\, 100$ Hz and, taking into account the frequency behavior of $\gamma(f)$ (see Fig. 1), we can assume $f_{\rm M} \,=\, 10$ kHz (i.e., $\nu_{\rm M} \,=\, 100$). The lower extreme $f_{\rm m}$ is put equal to the frequency f_b entering Eq. (2.1) (i.e., $\nu_{\rm m} \,=\, 0.02$).

For the chosen values of f_0 and S_0 (see Eq. (2.1)) one has:

$$h_0^2\,\overline{\Omega} \,\simeq\, \frac{4.0\,\times\,10^{-7}}{J}\,\left(\frac{1\ {\rm yr}}{T}\right)^{1/2}\,\mathrm{SNR}^2\,. \tag{2.4}$$

Since we will often refer to this formula we want to stress its physical meaning. Suppose that the functional form of $\omega(f)$ is given. Then the numerical value of the integral J can be precisely computed and, through Eq. (2.4), $\overline{\Omega}$ can be estimated. This quantity, inserted in Eq. (1.5), determines for each frequency f the minimum $\Omega_{\rm GW}$ detectable (for an observation time T, with a signal-to-noise ratio SNR) by the correlation of the two detector outputs.

In the next section, $\overline{\Omega}$ will be compared with two other quantities: $\overline{\Omega}^{\rm th}$ and $\overline{\Omega}^{\rm max}$. The first is the theoretical value of the normalization of the spectrum, while the second represents the largest normalization compatible with the phenomenological bounds applicable to the stochastic GW backgrounds. These quantities are of different nature and in order to be more precise let us consider an example.

Suppose, for simplicity, that we are dealing with a logarithmic energy spectrum which is a monotonic function of the present frequency. Suppose, moreover, that the spectrum decreases sufficiently fast in the infra-red in order to be compatible both with the pulsar timing bound and with the CMB anisotropies bounds. Then the most relevant bound will come, effectively, from Big-Bang nucleosynthesis (BBN) [22–24]. Therefore, in this particular case, we will have that $\overline{\Omega}^{\rm max}$ is determined by demanding that

$$h_0^2\,\int\,\Omega_{\rm GW}(f,\eta_0)\,{\rm d}\ln f\,<\,0.2\,h_0^2\,\Omega_\gamma(\eta_0)\,\simeq\,5\,\times\,10^{-6}, \tag{2.5}$$

where $\Omega_\gamma(\eta_0) \,=\, 2.6\,\times\,10^{-5}\,h_0^{-2}$ is the present fraction of critical energy density stored in radiation. According to our definition, $\overline{\Omega}^{\rm max}$ is the maximal normalization of the spectrum compatible with the previous inequality, namely,

$$h_0^2\,\overline{\Omega}^{\rm max} \,\simeq\, \frac{5\,\times\,10^{-6}}{\mathcal{I}}\,, \qquad \mathcal{I} \,=\, \int_{f_{\rm ns}}^{f_{\rm max}}\,\omega(f)\,{\rm d}\ln f. \tag{2.6}$$

Notice that $f_{\rm ns} \,\simeq\, 10^{-10}$ Hz is the present value of the frequency corresponding to the horizon at the nucleosynthesis time; $f_{\rm max}$ stands for the maximal frequency of the spectrum and it depends, in general, upon the specific theoretical model. If the spectrum has different slopes, $\overline{\Omega}^{\rm max}$ will be determined not only by the nucleosynthesis bound but also by the combined action of the CMB anisotropy bound [2,25] and of the pulsar timing bound [26]. Indeed, we know that the very small fractional timing error in the arrival times of the millisecond pulsar's pulses implies that $\Omega_{\rm GW} \lesssim 10^{-8}$ for a frequency which is roughly comparable with the inverse of the observation time along which pulsars have been monitored (i.e., $\omega_{\rm p} \,\sim\, 1/T_{\rm obs} \,=\, 10^{-8}$ Hz). Moreover, the observations of the large scale anisotropies in the microwave sky [25] imply that the graviton contribution to the integrated Sachs-Wolfe effect has to be smaller than (or at most of the order of) the detected amount of anisotropy. This observation implies that $\Omega_{\rm GW} \,\leq\, 6.9\,\times\,10^{-11}$ for frequencies ranging between the typical frequency of the present horizon and a frequency thirty of forty times larger. In the case of a logarithmic energy density with decreasing slope the $\overline{\Omega}^{\rm max}$ will be mainly determined by the Sachs-Wolfe bound and it will be the maximal normalization of the spectrum compatible with such a bound.

On a general ground, we will have that $\overline{\Omega}^{\rm th} \leq \overline{\Omega}^{\rm max}$, namely the theoretical normalization of the spectrum is bounded, from above, by the maximal normalization compatible with all the phenomenological bounds. Therefore, the mismatching between these quantities can be interpreted as an effective measure of the theoretical error in the determination of the absolute normalization of the spectrum.

Since $\omega(f)$ enters (in a highly non-linear way) into the form of J (as defined in Eq. (2.3)), the corresponding $\overline{\Omega}$ in Eq. (2.4) will be different for any (specific) frequency dependence in $\omega(f)$. The consequence of this statement is that it is not possible to give a general (and simple) relationship between the sensitivity at a given frequency, the spectral slope and the (generic) theoretical amplitude of the spectrum. However, given the form of the theoretical spectrum, the phenomenological bounds (depending upon the theoretical slope) will fix uniquely the theoretical error and the maximal achievable sensitivity. So, if we want to evaluate the performances of the VIRGO pair we should pick up a given class of theoretical models (characterized by a specific functional form of $\omega(f)$) and compute the corresponding sensitivity. The same procedure should then be repeated for other classes of models and, only at the end, the respective sensitivities can be compared.

III. PRIMORDIAL GRAVITON BACKGROUND VERSUS VIRGO*VIRGO

We can consider, in principle, logarithmic energy spectra with hypothetical analytical forms and arbitrary normalizations. If the logarithmic energy spectrum is either a flat or a decreasing function of the present frequency [6], we can expect, on general grounds, that the theoretical signal will be of the order of (but smaller than) 10^{-15} [27] for present frequencies comparable with the operating window of the VIRGO pair. This happens because of the combined action of the Sachs-Wolfe bound together with the spectral behavior of ther infra-red branch of the spectrum produced thanks to the matter-radiation transition. Of course this observation holds for models where the graviton production occurs because of the adiabatic variation of the background geometry [4].

In order to have large signals falling in the operating window of the VIRGO pair we should have deviations from scale invariance for frequencies larger than few mHz. Moreover, these deviations should go in the direction of increasing logarithmic energy spectra. This is what happens in the case of quintessential inflationary models [9]. In this case, however, as we discussed in a previous analysis [5], the BBN bound put strong constraints on the theoretical signal in the operating window of the VIRGO pair.

Another class of model leading to a large theoretical signal for frequencies between few Hz and 10 kHz is represented by string cosmological models [4,10,11]. Therefore, in order to evaluate the performances of the VIRGO pair and in order to implement a procedure of selective noise reduction we will use string cosmological spectra.

A. Minimal models of pre-big-bang

In string cosmology and, more specifically, in the pre-big-bang scenario, the curvature scale and the dilaton coupling are both growing in cosmic time. Therefore the graviton spectra will be *increasing* in frequency instead of *decreasing* as it happens in ordinary inflationary models.

In the context of string cosmological scenarios the Universe starts its evolution in a very weakly coupled regime with vanishing curvature and dilaton coupling. After a phase of sudden growth of the curvature and of the coupling the corrections to the tree level action become important and the Universe enters a true stringy phase which is followed by the ordinary radiation dominated phase. It should be stressed that the duration of the stringy phase is not precisely known and it could happen that all the physical scales contained within our present Hubble radius crossed the horizon during the stringy phase as pointed out in [31].

The maximal amplified frequency of the graviton spectrum is given by [4,11]

$$f_1(\eta_0) \simeq 64.8\,\sqrt{g_1}\left(\frac{10^3}{n_r}\right)^{1/12}\ {\rm GHz} \tag{3.1}$$

where n_r is the effective number of spin degrees of freedom in thermal equilibrium at the end of the stringy phase, and $g_1 = M_s/M_{\rm Pl}$ where M_s and $M_{\rm Pl}$ are the string and Planck masses, respectively. Notice that g_1 is the value

[4] An exception to this assessment is represented by cosmic strings models leading to a flat logarithmic energy spectrum for frequencies between 10^{-12} Hz and 10^{-8} Hz [28]. Another possible exception is given by the gravitational power radiated by magnetic (and hypermagnetic) [29] knot configurations at the electroweak scale [30].

of the dilaton coupling at the end of the stringy phase, and is typically of the order of $10^{-2} \div 10^{-1}$ [32]. In order to red-shift the maximal amplified frequency of the spectrum from the time η_1 (which marks the beginning of the radiation dominated evolution) up to the present time we assumed that the cosmological evolution prior to η_0 and after η_1 is adiabatic. Minimal models of pre-big-bang are the ones where a dilaton dominated phase is followed by a stringy phase which terminates at the onset of the radiation dominated evolution. In the context of minimal models, the function $\omega(f)$ introduced in Eq. (1.5) can be written as

$$\omega(f) = \begin{cases} z_s^{-2\beta} \left(\frac{f}{f_s}\right)^3 \left[1 + z_s^{2\beta-3} - \frac{1}{2}\ln\frac{f}{f_s}\right]^2 & f \leq f_s = \frac{f_1}{z_s} \\ \left[\left(\frac{f}{f_1}\right)^{3-\beta} + \left(\frac{f}{f_1}\right)^{\beta}\right]^2 & f_s < f \leq f_1 \end{cases} \tag{3.2}$$

where,

$$\beta = \frac{\ln(g_1/g_s)}{\ln z_s}. \tag{3.3}$$

In this formula $z_s = f_1/f_s$ and g_s are, respectively, the red-shift during the string phase and the value of the coupling constant at the end of the dilaton dominated phase. The first of the two branches appearing in Eq. (3.2) is originated by modes leaving the horizon during the dilaton dominated phase and re-entering during the radiation dominated phase. The second branch is mainly originated by modes leaving the horizon during the stringy phase and re-entering always in the radiation dominated phase. The theoretical normalization

$$\overline{\Omega}^{\rm th} = 2.6\, g_1^2 \left(\frac{10^3}{n_r}\right)^{1/3} \Omega_\gamma(\eta_0)\,, \tag{3.4}$$

multiplied by $\omega(f)$ (as given in Eq. (3.2)) leads to the theoretical form of the spectrum. Notice that n_r is of the order of $10^2 \div 10^3$ (depending upon the specific string model) and it represents a theoretical uncertainty.

However, as anticipated in the previous section, the theoretical normalization of the spectrum should be contrasted with the one saturating the BBN bound (i.e., $\overline{\Omega}^{\rm max}$). This quantity is obtained by Eq. (2.6), where in the case under consideration

$$\mathcal{I} = \mathcal{I}_d + \mathcal{I}_s \qquad \text{with} \qquad \mathcal{I}_d = \int_{f_{\rm ns}}^{f_s} \frac{{\rm d}f}{f}\,\omega(f)\,, \qquad \mathcal{I}_s = \int_{f_s}^{f_1} \frac{{\rm d}f}{f}\,\omega(f)\,. \tag{3.5}$$

The analytical expressions of $\mathcal{I}_d$ and $\mathcal{I}_s$ are reported in Appendix B. We have to bear in mind that in the intermediate frequency region of the graviton spectra an important bound comes from the pulsar timing measurements. Therefore, if one ought to consider rather long stringy phases (i.e., large z_s), the BBN constraint should be supplemented by the requirement that $\Omega_{\rm GW}(10^{-8}\,{\rm Hz}) < 10^{-8}$ [26]. We will come back to this point later.

Following the explicit expression of the function $\omega(f)$, Eq. (2.4) can be re-written as follows:

$$h_0^2\,\overline{\Omega} \simeq 4 \times 10^{-7} \left(\frac{1\,{\rm yr}}{T}\right)^{1/2} \frac{{\rm SNR}^2}{\sqrt{J_d^2 + J_s^2}}, \tag{3.6}$$

where, introduced the following notation

$$J_k = \int_{\nu_{\rm m}}^{\nu_s} {\rm d}\nu\, \frac{\gamma^2(f_0\nu)}{\Sigma_n^{(1)}(f_0\nu)\,\Sigma_n^{(2)}(f_0\nu)}\,\ln^k\nu\,, \qquad k = 0,1,2,3,4$$

$$J_{\pm m(3-2\beta)} = \int_{\nu_s}^{\nu_{\rm M}} {\rm d}\nu\, \frac{\gamma^2(f_0\nu)}{\Sigma_n^{(1)}(f_0\nu)\,\Sigma_n^{(2)}(f_0\nu)}\,\nu^{\pm m(3-2\beta)}\,, \qquad m = 1,2 \tag{3.7}$$

$$C_d = 1 + z_s^{2\beta-3} + \frac{1}{2}\ln\nu_s\,,$$

one has

$$J_d = \frac{z_s^{3-2\beta}}{\nu_1^3}\left(C_d^4 J_0 - 2C_d^3 J_1 + \frac{3}{2}C_d^2 J_2 - \frac{1}{2}C_d J_3 + \frac{1}{16}J_4\right)^{1/2},$$

$$J_s = \frac{1}{\nu_1^3}\left(6J_0 + \frac{J_{6-4\beta}}{\nu_1^{6-4\beta}} + \frac{J_{4\beta-6}}{\nu_1^{4\beta-6}} + 4\frac{J_{3-2\beta}}{\nu_1^{3-2\beta}} + 4\frac{J_{2\beta-3}}{\nu_1^{2\beta-3}}\right)^{1/2}. \tag{3.8}$$

The previous expressions are general in the sense that they are applicable for a generic value of f_s. If $f_{\rm m} < f_s < f_{\rm M}$ then both J_s and J_d give contribution to the sensitivity. If, on the other hand $f_s < f_{\rm m}$ (i.e., a long stringy phase) the main contribution to the sensitivity will come from J_s. The integrals appearing in $J_{d,s}$ have to be evaluated numerically. In all our calculations we will assume that both VIRGO detectors are characterized by the same (rescaled) NPS (reported in Eq. (2.2)).

The main steps of our calculation are the following. We firstly fix g_1 and for each pair (z_s, g_1/g_s) (within the range of their physical value) we compute $\overline{\Omega}$ (for $T = 1$ yr and SNR $= 1$), and $\overline{\Omega}^{\rm max}$. We then compare these two quantities to the theoretical normalization given in Eq. (3.4). If $\overline{\Omega}^{\rm th}$ will be larger than $\overline{\Omega}$ (but smaller than $\overline{\Omega}^{\rm max}$) we will say that the theoretical signal will be "visible" by the VIRGO pair. In this way we will identify in the plane (z_s, g_1/g_s) a visibility region according to the sensitivity of the VIRGO pair. The theoretical error on the border of this region can be estimated by substituting $\overline{\Omega}^{\rm max}$ to $\overline{\Omega}^{\rm th}$.

To illustrate this point we consider a specific case. The value of the coupling at the end of the stringy phase can be estimated to lie between 0.3 and 0.03 [32]. The knowledge of g_1 will not fix uniquely the theoretical spectrum which does also depend on the number of relativistic degrees of freedom at the end of the stringy phase. Therefore, the theoretical error in the determination of the absolute normalization of the spectrum could be also viewed as the error affecting the determination of n_r. In all the plots shown we will take, when not otherwise stated, $g_1 = 1/20$ and $n_r = 10^3$ as fiducial values. Different choices of g_1 will lead to similar results. We will also assume that the overlap reduction function associated with the pair is the one reported in the curve A of Fig. 1.

In Fig. 2 (top left) we report the result of our calculation for the ratio between $\overline{\Omega}^{\rm max}$ and $\overline{\Omega}$ as a function of g_1/g_s and $\log z_s$. The contour plot (bottom left) shows the region of the plane ($\log z_s$, g_1/g_s) where this ratio is greater than 1, i.e. the maximal visibility region allowed by the BBN bound. In the opposite case, i.e., $\overline{\Omega}^{\rm max}/\overline{\Omega} < 1$, the VIRGO pair is sensitive to a region excluded by the BBN. In the right part of Fig. 2 we go one step further and we plot the ratio between $\overline{\Omega}^{\rm th}$ and $\overline{\Omega}$. The shaded area in the contour plot (bottom right) is the region of the plane ($\log z_s$, g_1/g_s) where the conditions $\overline{\Omega}^{\rm th}/\overline{\Omega} > 1$ and $\overline{\Omega}^{\rm max}/\overline{\Omega} > 1$ are simultaneously met. The shaded area in this plot defines the visibility region of the VIRGO pair *assuming* the theoretical normalization of the spectrum. From Fig. 2, by ideally subtracting the shaded area of the left contour plot from the shaded area of the right contour plot we obtain an estimate of the theoretical error. The results we just presented can be obviously recovered for different values of g_1 close to one. However, if g_1 gets too small (and typically below 1/25) the visibility area gets smaller and smaller eventually disappearing.

The visibility regions appearing in Fig. 2 extend from intermediate values of z_s (of the order of 10^8) towards large values of z_s (of the order of 10^{18}). Notice that for our choice of g_1, f_s can become as small as 10^{-8} for z_s of the order of 10^{18}. As we recalled in the previous Section, this frequency corresponds to the inverse of the observation time along which pulsar signals have been monitored and, therefore, for this frequency, a further "local" bound applies to the logarithmic energy spectra of relic gravitons. This bound implies that $\Omega_{\rm GW}(10^{-8}\,{\rm Hz}) < 10^{-8}$. In our examples, the compatibility with the BBN bound implies also that the pulsar timing constraint is satisfied. Given our choice for g_1 we can clearly see that the visibility regions depicted in Fig. 2 extend for values of g_s which can be as small as 1/160 (or as small as 1/60 in the case of right part of Fig. 2).

B. Non-minimal models of pre-big-bang

In the context of minimal models of pre-big-bang, the end of the stringy phase coincides with the onset of the radiation dominated evolution. At the moment of the transition to the radiation dominated phase the dilaton seats at its constant value. This means that $g_1 \sim 0.03 \div 0.3$ at the beginning of the radiation dominated evolution. As pointed out in [31], it is not be impossible to imagine a scenario where the coupling constant is still growing while the curvature scale starts decreasing in time. In this type of scenario the stringy phase is followed by a phase where the dilaton still increases, or, in other words, the coupling constant is rather small at the moment where the curvature starts decreasing so that $g_1 \ll 1$.

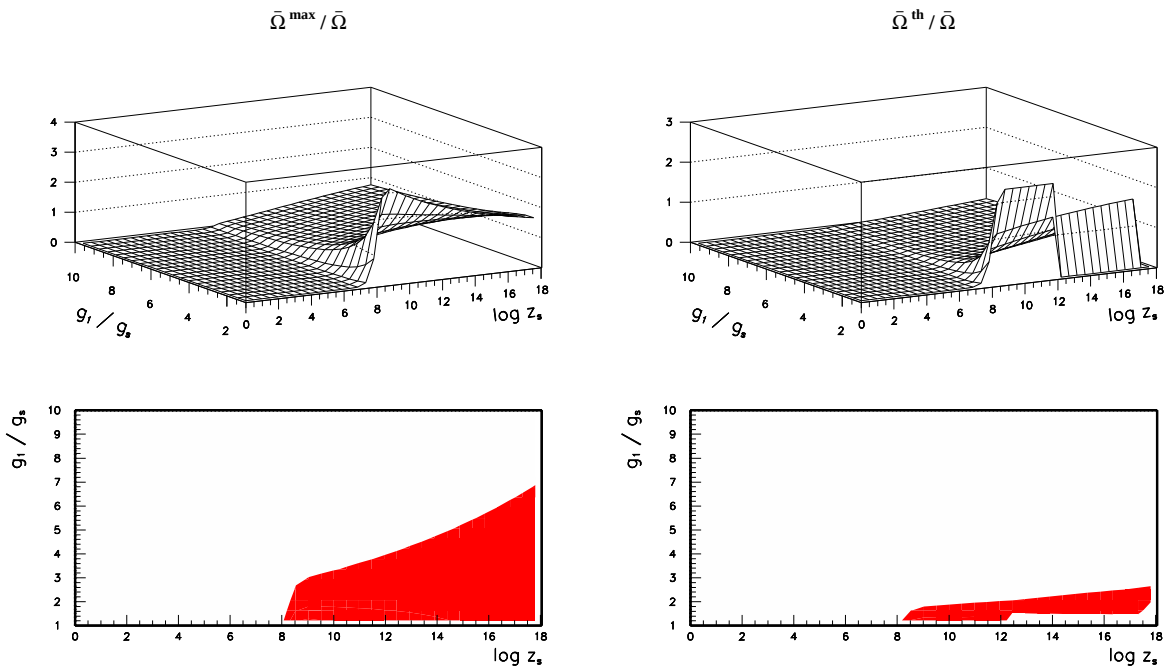

FIG. 2. We report the ratios $\overline{\Omega}^{\rm max}/\overline{\Omega}$ (left) and $\overline{\Omega}^{\rm th}/\overline{\Omega}$ (right) as a function of g_1/g_s and $\log z_s$ ($\overline{\Omega}$ is calculated for $T = 1$ yr and SNR = 1). The lower contour plots show the regions where these ratios are greater than 1. The shaded area (bottom right) represents the region where the combination of the theoretical parameters is such that the corresponding $\overline{\Omega}^{\rm th}$ does not violate the BBN bound. As we can see the visibility region is reduced. The difference between the shaded area in the right plot and the one in the left plot measures the error made by assuming as normalization of the spectrum not the theoretical one but the maximal one compatible with the BBN. The value $z_s = 10^8$ roughly corresponds to $f_s \sim f_0$. Notice that log denotes not the Neperian logarithm but the logarithm in ten basis.

After a transient period (whose precise duration will be fixed by the value of g_1), we will have that the radiation dominated evolution will take place when the value of the coupling constant will be of order one (i.e., $g_r \sim 1$).

An interesting feature of this speculation is that the graviton spectra will not necessarily be monotonic [31] (as the ones considered in the previous analysis). We then find interesting to apply our considerations also to this case.

The function $\omega(f)$ in the non-minimal model described above is given by [31] [5]

$$\omega(f) = \begin{cases} \left(\frac{g_r}{g_1}\right)^{2/\sqrt{3}} \left(\frac{f}{f_1}\right)^4 \left[\left(\frac{f_s}{f_1}\right)^{-\sigma} + \left(\frac{f_s}{f_1}\right)^{\sigma}\right]^2 \left(1 - \ln\frac{f_s}{f_1}\right)^2 & f_r < f \leq f_s = \frac{f_1}{z_s} \\ \left(\frac{g_r}{g_1}\right)^{2/\sqrt{3}} \left[\left(\frac{f}{f_1}\right)^{2-\sigma} + \left(\frac{f}{f_1}\right)^{2+\sigma}\right]^2 \left(1 - \ln\frac{f}{f_1}\right)^2 & f_s < f \leq f_1 \end{cases} \tag{3.9}$$

where, in the present case

$$f_1 \simeq 64.8\,\sqrt{g_1}\left(\frac{g_r}{g_1}\right)^{1/2\sqrt{3}}\left(\frac{10^3}{n_r}\right)^{1/12}\,{\rm GHz}\,, \qquad f_r = \left(\frac{g_r}{g_1}\right)^{-2/\sqrt{3}} f_1\,. \tag{3.10}$$

The frequency f_r corresponds to the onset of the radiation dominated evolution. If we adopt a purely phenomenological approach we can say that f_r has to be bounded (from below) since we want the Universe to be radiation dominated

[5] Notice that the form of $\omega(f)$ reported in [31] differs from our expression only by logarithmic correction whose presence is, indeed, not relevant. We kept them only for sake of completeness.

not later than the BBN epoch. Thence, we have that $f_r > f_{\rm ns}$. Recalling the value of the nucleosynthesis frequency and assuming that $g_r \simeq 1$ this condition implies $g_1 \gtrsim 8.2 \times 10^{-16}$. This simply means that in order not to conflict with the correct abundances of the light elements we have to require that the coupling constant should not be too small when the curvature starts decreasing. Notice that for frequencies $f < f_r$ the spectrum evolves as f^{-3}. The ultra-violet branch of the spectrum is mainly originated by modes leaving the horizon during the stringy phase and re-entering when the dilaton coupling is still increasing.

Concerning the non-minimal spectra few comments are in order. Owing to the fact that g_1 can be as small as 10^{-15} we have that the highest frequency of the spectrum can become substantially smaller than in the minimal case. Moreover, the spectrum might also be non-monotonic with a peak at f_s. Looking at the analytical form of the spectrum we see that this behavior occurs if $\sigma > 2$. A non-monotonic logarithmic energy spectrum (with a maximum falling in the sensitivity region of the VIRGO pair) represents an interesting possibility.

The results of our calculation for $g_1 = 10^{-12}$, $n_r = 10^3$, $g_r = 1$,and $\sigma > 2$ are reported in Fig. 3. As done in the case of minimal spectra we analyse the visibility window in the plane of the relevant parameters of the model. As we can see from the left part of Fig. 3 the region compatible with the BBN is rather large but it shrinks when we impose the theoretical normalization (right part of Fig. 3) which is always smaller than the maximal normalization allowed by BBN.

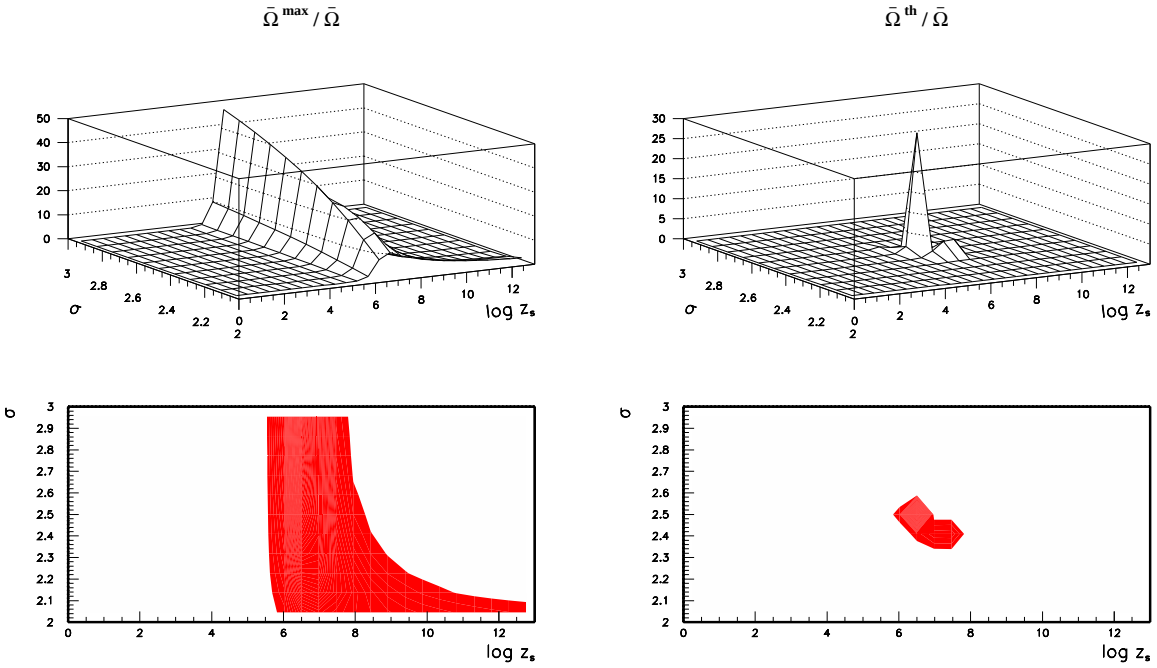

FIG. 3. In order to make clear the comparison with the visibility region of the minimal models, we report $\overline{\Omega}^{\rm max}/\overline{\Omega}$ (left) and $\overline{\Omega}^{\rm th}/\overline{\Omega}$ (right) as a function of σ and of the $\log z_s$ in the non-minimal scenario. Notice that we took $g_1 = 10^{-12}$, $n_r = 10^3$, and $g_r = 1$. As for Fig. 2, the shaded areas in the lower contour plots represent the region where each ratio is greater than 1, and, in the case of the right plot, also the BBN is satisfied.

It is interesting to compare directly the three dimensional plots appearing in Fig. 2 with the corresponding three dimensional plots of Fig. 3. We can see that the regions of parameter space where $\overline{\Omega}^{\rm max}/\overline{\Omega}$ and $\overline{\Omega}^{\rm th}/\overline{\Omega}$ are larger than one is larger in the case of minimal models. However, the shaded region in the case of minimal models corresponds to ratios $\overline{\Omega}^{\rm max}/\overline{\Omega}$ and $\overline{\Omega}^{\rm th}/\overline{\Omega}$ which can be 3 or 2, respectively. On the other hand the shaded region in the case of Fig. 3 corresponds to ratios $\overline{\Omega}^{\rm max}/\overline{\Omega}$ and $\overline{\Omega}^{\rm th}/\overline{\Omega}$ which can be, respectively, as large as 50 or 25. So, in the latter case the signal is larger for a smaller region of the parameter space.

As we stressed in the previous Section, $\overline{\Omega}$ represents the sensitivity of the VIRGO pair to a given spectrum whose functional form is given by $\omega(f)$. One might be interested, in principle, in the sensitivity of the VIRGO pair at a specific frequency f^*. This can be easily computed by multiplying $\overline{\Omega}$ by $\omega(f^*)$. In Fig. 4 we show the sensitivity of the VIRGO pair at the frequency $f^* = 100$ Hz, both, for the minimal and non-minimal models considered in the

present Section. One can easily discuss the same quantity for any other frequency in the operating window of the VIRGO detectors.

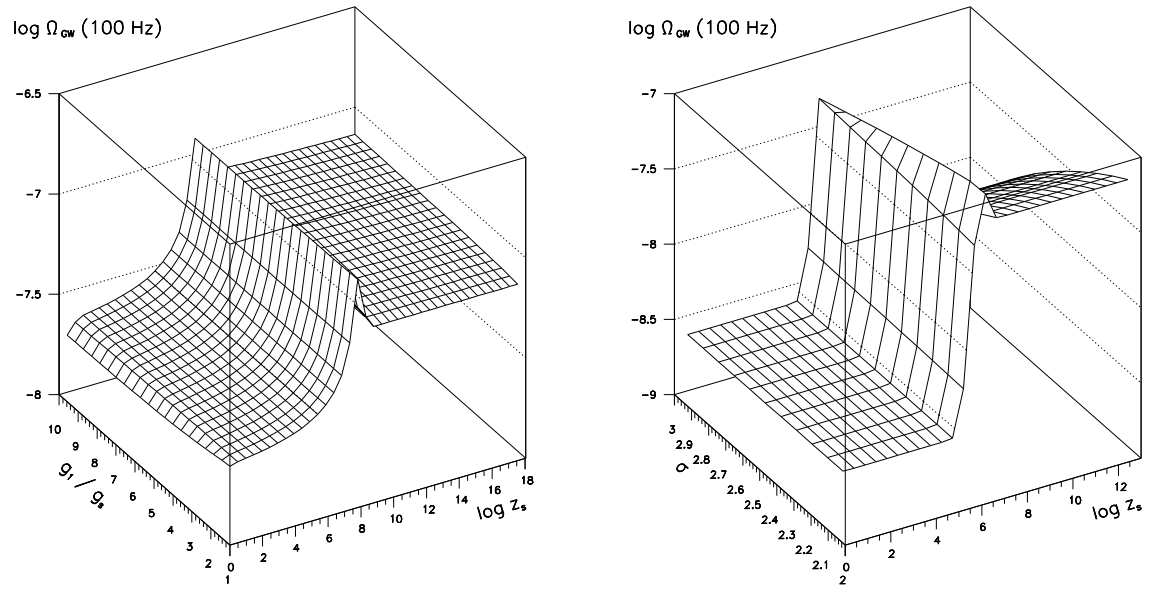

FIG. 4. We report the logarithm of the sensitivity of the VIRGO pair at 100 Hz for $T = 1$ yr and SNR = 1 in the case of minimal (left plot) and non-minimal (right plot) energy spectra.

IV. NOISE REDUCTION AND THE VISIBILITY REGION OF A VIRGO PAIR

There are two ways of looking at the calculations reported in this paper. One can look at these ideas from a purely theoretical perspective. In this respect we presented a study of the sensitivity of a pair of VIRGO detectors to string cosmological gravitons. There is also a second way of looking at our exercise. Let us take at face value the results we obtained and let us ask in what way we can enlarge the visibility region of the VIRGO pair. In this type of approach the specific form of graviton spectrum is not strictly essential. We could use, in principle, any motivated theoretical spectrum. As we stressed, we will use string cosmological spectra because, on one hand, they are theoretically motivated and, on the other hand, they give us a signal which could be, in principle detected. Of course, there are other well motivated spectra (like the ones provided by ordinary inflationary models). However, the signal would be, to begin with, quite small.

In this Section we will then consider the following problem. Given a pair of VIRGO detectors, we suppose to be able, by some means, to reduce, in a selective fashion, the contribution of a specific noise source to the detectors output. The question we ought to address is how the visibility regions will be modified with respect to the case in which the selective noise reduction is not present. We will study the problem for the pair of VIRGO detectors considered in the previous Sections, i.e., for identical detectors with NPS given in Eq. (2.1), and characterized by the overlap reduction function of the case A of Fig. 1. As for the theoretical graviton spectrum we will focus our attention on the case of minimal models considered in Section III.A, with the same parameters used to produce Fig. 2. Also here, the quantity $\overline{\Omega}$ will be computed for $T = 1$ yr and SNR = 1.

As shown in Section II the NPS is characterized by three dimension-less numbers $\Sigma_{1,2,3}$, and two frequencies f_a and f_b. Roughly, Σ_1 and Σ_2 control, respectively, the strength of the pendulum and pendulum's internal modes noise, whereas Σ_3 is related to the shot noise (see Ref. [33] for an accurate description of the phenomena responsible of these noises). Below the frequency f_b the NPS is dominated by the seismic noise (assumed to be infinitum in Eq. (2.1)). The frequency f_a is, roughly, where the NPS gets its minimum. The frequency behavior of this three contributions

and of the total NPS is shown in Fig. 5. The stochastic processes associated with each source of noise are assumed to be Gaussian and stationary.

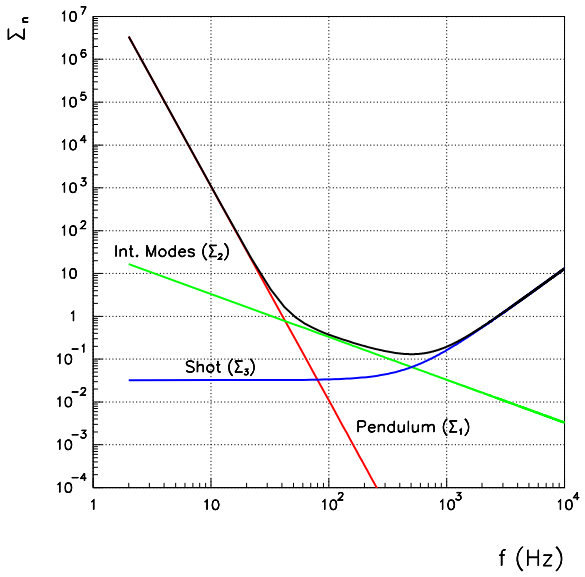

FIG. 5. The analytical fit of the rescaled noise power spectrum Σ_n defined in Eq. (2.1) in the case of the VIRGO detector. With the full (thick) line we denote the total NPS. We also report the separated contribution of the three main (Gaussian and stationary) sources of noise.

In the following, without entering in details concerning the actual experimental strategy adopted for the noise reduction, we will suppose to be able to reduce each of the coefficients Σ_i by keeping the other fixed. In order to make our notation simpler we define a "reduction vector"

$$\vec{\rho} = (\rho_1, \rho_2, \rho_3) \, , \tag{3.1}$$

whose components define the reduction, respectively, of the seismic, thermal and shot noises with respect to their fiducial values appearing in Eq. (2.1) (corresponding to the case $\vec{\rho} = (1, 1, 1)$).

As shown in Fig. 5 the pendulum noise dominates the sensitivity of the detectors in the low frequency region, namely below about 40 Hz. In Fig. 6 we report the results of our calculation for the case $\vec{\rho} = (0.1, 1, 1)$. Here the parameters of the theoretical spectrum are exactly the same as in Fig. 2. The only change is given by a reduction of the pendulum noise. From the comparison between Fig. 6 and Fig. 2, we see that the visibility region in the parameter space of our model gets immediately larger especially towards the region of small g_s. This enlargement is quite interesting especially in terms of $\overline{\Omega}^{\rm th}/\overline{\Omega}$.

In the frequency region between 50 and 500 Hz the performances of the detectors are, essentially, limited by the pendulum's internal modes noise. The results obtained for a selective reduction of this component are summarized in Fig. 7, where the pendulum and shot noises are left unchanged but the internal modes component is reduced by a factor of ten (in Fig. 8). As we can see the visibility region gets larger and the increase in the area is comparable with the one obtained by selecting only the pendulum noise.

Finally, for sake of completeness, we want to discuss the case of the shot noise, i.e., the noise characteristic of the detector above 500 Hz. Our results for $\rho_3 = 0.1$ are reported in Fig. 9. As we can see by comparing Figs. 6, 7, and 8 we gain much more in visibility by reducing the thermal noise components than by reducing the shot noise. In Fig. 8 the shot noise is reduced by one tenth but the visibility region does not increase by much (left plot). This result is consequence of the fact that, as shown by Fig. 5, the shot noise contribution to the NPS starts to be relevant for $f \sim 1$ kHz, i.e., in a frequency region where the overlap between the detectors begins to deteriorate (see Fig. 1). In Figs. 6 and 7 the thermal noise is reduced by one tenth and the increase in the visibility region is, comparatively, larger. This shows, amusingly enough, that a reduction in the shot noise will lead to an effect whose practical relevance is already questionable at the level of our analysis. Notice that a selective noise reduction can be also discussed in the case of a purely flat spectrum [20].

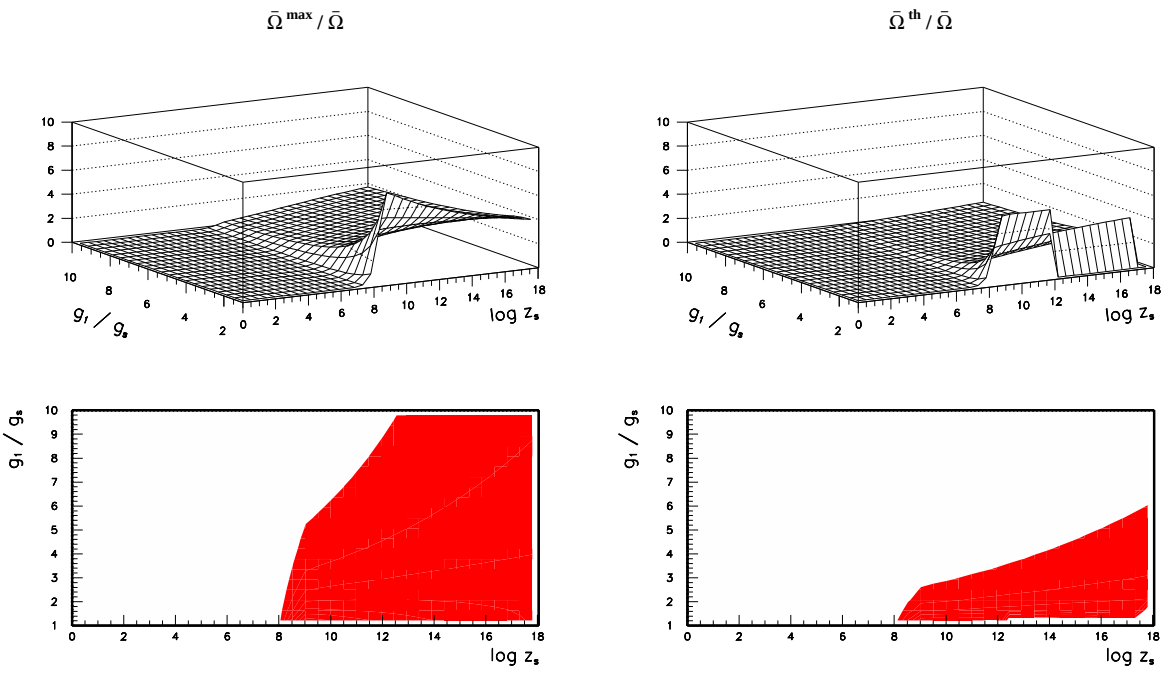

FIG. 6. We report the ratios $\overline{\Omega}^{\max}/\overline{\Omega}$ (left plots), and $\overline{\Omega}^{\rm th}/\overline{\Omega}$ (right plots) in the case in which the shot noise and the noise related to the pendulum's internal modes are not reduced, whereas the pendulum noise is diminished by a factor of ten with respect to the values quoted in Eq. (2.1), i.e., $\vec{\rho} = (0.1, 1, 1)$.

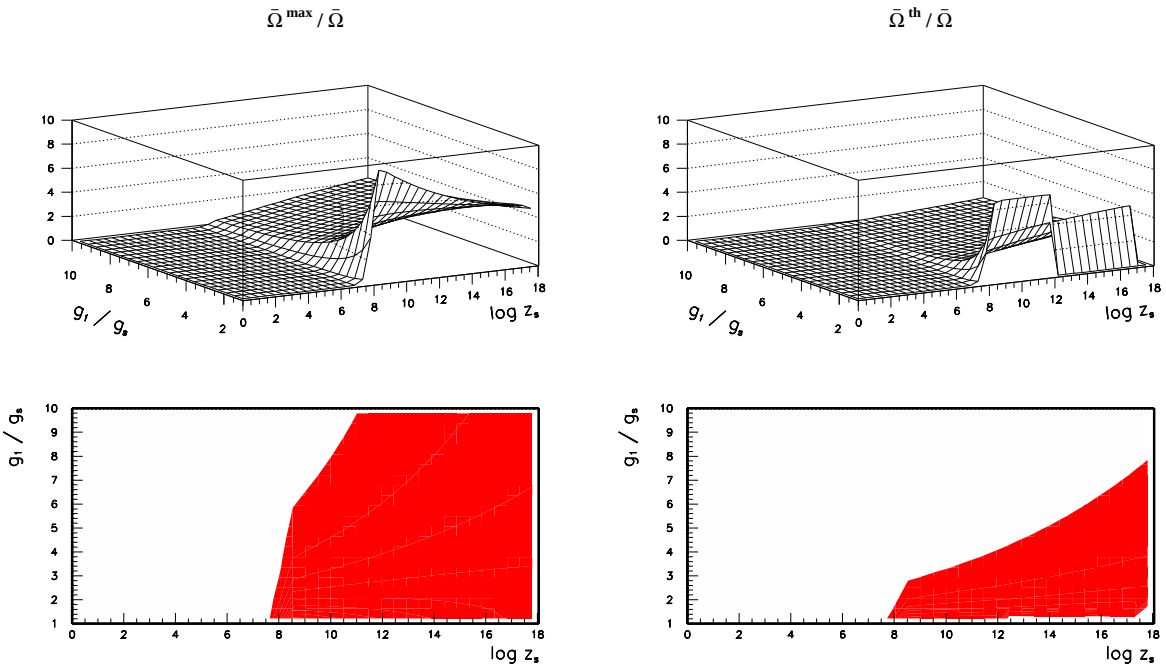

FIG. 7. We report the result of selective reduction in the case where the noise cause by the pendulum's internal modes is reduced by a factor of ten, whereas the pendulum and shot contributions are left unchanged, i.e., $\vec{\rho} = (1, 0.1, 1)$.

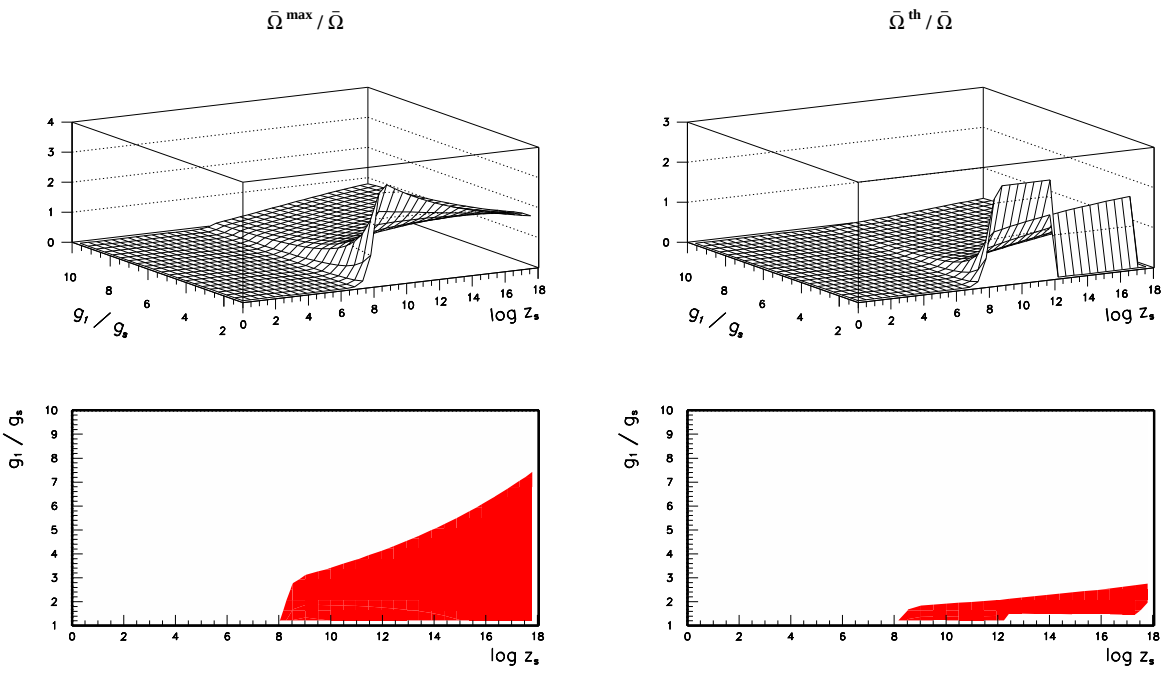

FIG. 8. We report the same quantities discussed in Fig. 6 for the case $\vec{\rho} = (1, 1, 0.1)$. Thhe shaded areas in the lower plots are the relevant visibility regions which should be compared with the shaded regions in the lower plots of Figs. 6 and 7. By direct comparison we can argue that a reduction in the shot noise (by a factor of ten) is not as efficient as a reduction, by the same amount, in the thermal noise components.

In order to conclude this Section we want to show the combined action of the simultaneous reduction of both the components of the thermal noise. In Fig. 9, owing to the results of our analysis we kept the shot noise fixed but we reduced both the thermal and seismic noises by a factor of ten. Clearly we observe a consistent increase in the visibility region. However, even if a combined reduction of these components cannot be achieved we want to stress that already a reduction of the pendulum's internal modes noise alone (by one tenth) can be of relevant practical interest.

V. DISCUSSION AND EXECUTIVE SUMMARY

There are no compelling reasons why one should not consider the appealing theoretical possibility of a second VIRGO detector coaligned with the first one. Moreover, recent experimental suggestions seem coherently directed towards this goal [19]. While the location of the second detector is still under debate we presented a theoretical analysis of some of the scientific opportunities suggested by this proposal.

We focused our attention on possible cosmological sources of relic gravitons and we limited our attention to the case of stochastic and isotropic background produced by the adiabatic variation of the backgound geometry. In the framework of these models we can certainly argue that in order to have a large signal in the frequency window covered by VIRGO we have to focus our attention on models where the logarithmic energy spectrum increases at large frequencies. Alternatively we have to look for models where the logarithmic energy spectrum exhibits some bump in the vicinity of the VIRGO operating window. If the logarithmic energy spectra are decreasing as a function of the present frequency (as it happens in ordinary inflationary models) the large scale (CMB) constraints forbid a large signal at high frequencies. In the case of string cosmological models the situation seems more rosy and, therefore, we use these models as a theoretical laboratory in order to investigate, in a specific model the possible improvements of a possible VIRGO pair. The choice of a specific model is, in some sense, mandatory. In fact, owing to the form of the SNR we can immediately see that different models lead to different SNR not only because the amplitude of the signal differs in different models. Indeed, one can convince himself that two models with the same amplitude at 100 Hz but different spectral behaviors between 2 Hz and 10 kHz lead to different SNR.

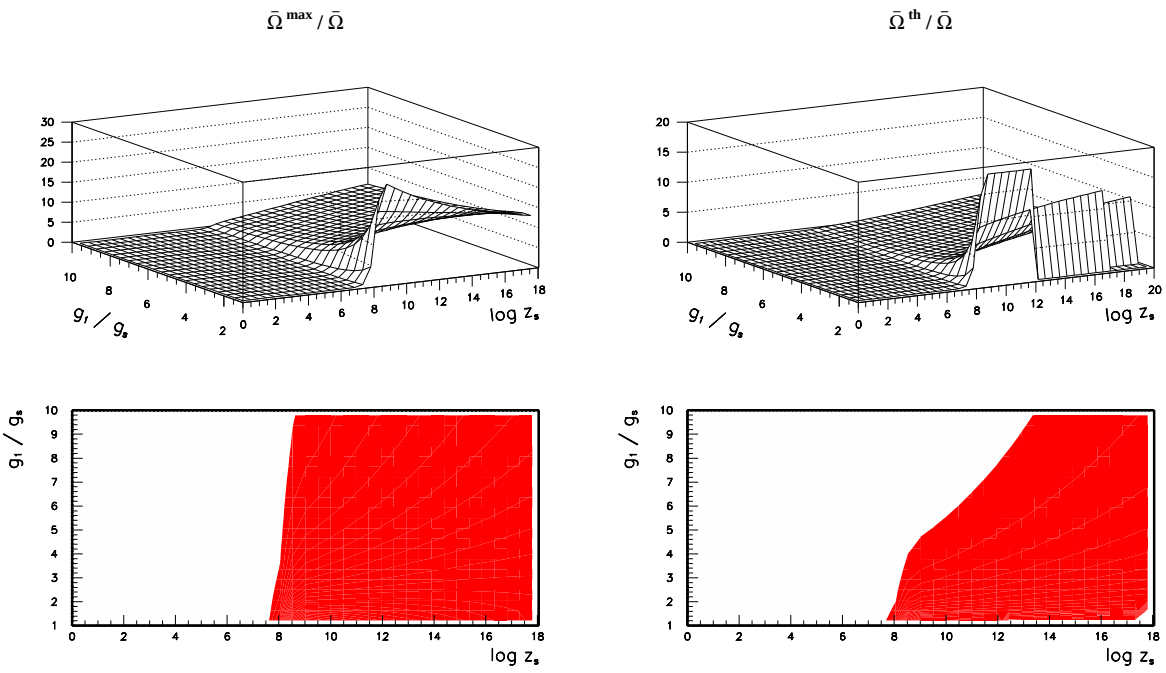

FIG. 9. We illustrate the case of a simultaneous reduction of Σ_1 and Σ_2 by a factor 10, whereas Σ_3 is the same of Eq. (2.1), i.e., $\vec{\rho} = (0.1, 0.1, 1)$.

In order to analyze the sensitivity of the VIRGO pair we described a semi-analytical technique whose main advantage is to produce the sensitivity of the VIRGO pair to a theoretical spectrum of arbitrary slopes and amplitudes. The theoretical error is estimated, in our approach, by requiring the compatibility with all the phenomenological bounds applicable to the graviton spectra. As an intersting example, we asked what is the sensitivity of a VIRGO pair to string cosmological spectra *assuming* that a second VIRGO detector (coaligned with the first one) is built in a european site. By assuming that the second VIRGO detector has the same features of the first one we computed the SNR and the related sensitivity achievable after one year of observation in the case of string cosmological spectra.

By using the string cosmological spectra as a theoretical laboratory we then studied some possible noise reduction. Our main goal, in this respect, has been to spot what kind of stationary and stochastic noise should be reduced in order to increase the visibility region of the VIRGO pair in the parameter space of the theoretical models under considerations. Our main result is that a selective reduction of each of the three main sources of noise is not equivalent. A reduction in the shot noise by a factor of ten does not increase significantly the visibility region of the VIRGO pair. A selective reduction of the thermal noise components is far more efficient. In particular, we could see that a reduction (of one tenth) of the pendulum's internal modes increases the visibility region of four times. The simultaneous reduction of the two components of the thermal noise leads to an even more relevant increase.

The construction of a second VIRGO detector coaligned with the first one and an overall reduction of the thermal noise of each detector of the pair leads to what we called "upgraded VIRGO" program. The results presented in this paper are obtained in the case of a particularly promising class of theoretical models but can be generally applied to any logarithmic energy spectrum with similar qualitative results. However, owing to the non-linearities present in the evaluation of the SNR it would not be correct assess that they hold, quantitatively, without change. We hope that our results and our suggestions may turn out to be useful in the actual process of design of the upgraded VIRGO program [19].

ACKNOWLEDGEMENTS

We would like to thank A. Giazotto for very useful hints and for his kind interest in this investigation.

APPENDIX A: THE NORMALIZATION OF THE OVERLAP REDUCTION FUNCTION

In this Appendix we discuss the reduction in sensitivity due to the fact that, in general, these detectors will not be either coincident or coaligned. This effect is quantified by the (dimensionless) overlap reduction function $\gamma(f)$ appearing in Eq. (1.4). Suppose that we have a gravitational wave propagating along a generic direction characterized, in spherical coordinates, by the unit vector $\hat{\Omega} = (\cos\phi\,\sin\theta,\,\sin\phi\,\sin\theta,\,\cos\theta)$. If we now introduce a pair of orthogonal unit vectors directed in the plane perpendicular to $\hat{\Omega}$

$$\hat{m}(\hat{\Omega}) \equiv (\cos\phi\,\cos\theta,\,\sin\phi\,\cos\theta,\,-\sin\theta) \qquad\qquad \hat{n}(\hat{\Omega}) \equiv (\sin\phi,\,-\cos\phi,\,0)\,, \tag{B.1}$$

the polarization tensors can be written, in terms of the polarization angle ψ of the GW, as

$$\begin{aligned} \varepsilon^{+}(\hat{\Omega},\psi) &= e^{+}(\hat{\Omega})\cos 2\psi \;-\; e^{\times}(\hat{\Omega})\sin 2\psi \\ \varepsilon^{\times}(\hat{\Omega},\psi) &= e^{+}(\hat{\Omega})\sin 2\psi \;+\; e^{\times}(\hat{\Omega})\cos 2\psi\,, \end{aligned} \tag{B.2}$$

where

$$e^{+}(\hat{\Omega}) = \hat{m}(\hat{\Omega})\otimes\hat{m}(\hat{\Omega}) - \hat{n}(\hat{\Omega})\otimes\hat{n}(\hat{\Omega}) \qquad e^{\times}(\hat{\Omega}) = \hat{m}(\hat{\Omega})\otimes\hat{n}(\hat{\Omega}) + \hat{n}(\hat{\Omega})\otimes\hat{m}(\hat{\Omega}) \tag{B.3}$$

with the normalization

$$\mathrm{Tr}\,\{e^{A}(\hat{\Omega})\,e^{A'}(\hat{\Omega})\} = 2\,\delta^{AA'}\,.$$

If the graviton background is isotropic and unpolarized we will have that

$$\gamma(f) = \frac{1}{F}\sum_{A} < e^{i2\pi f\hat{\Omega}\cdot\Delta\vec{r}}\,F_1^A(\hat{r}_1,\hat{\Omega},\psi)F_2^A(\hat{r}_2,\hat{\Omega},\psi) >_{\hat{\Omega},\psi} = \frac{\Gamma(f)}{F} \tag{B.4}$$

where $\Delta\vec{r} = \vec{r}_1 - \vec{r}_2$ is the separation vector between the two detector sites, F_i^A is the pattern function characterizing the response of the i-th detector ($i = 1, 2$) to the $A = +, \times$ polarization, and the following notation

$$< ... >_{\hat{\Omega},\psi} = \int_{S^2}\frac{\mathrm{d}\hat{\Omega}}{4\pi}\int_0^{2\pi}\frac{\mathrm{d}\psi}{2\pi}\,(...) \tag{B.5}$$

has been introduced to indicate the average over the propagation direction (θ,ϕ) and the polarization angle ψ. The normalization factor F is given by:

$$F = \sum_{A} < F_1^A(\hat{r}_1,\hat{\Omega},\psi)F_2^A(\hat{r}_2,\hat{\Omega},\psi) >_{\hat{\Omega},\psi}|_{1\equiv 2}\,, \tag{B.6}$$

where the notation $1 \equiv 2$ is a compact way to indicate that the detectors are coincident and coaligned and, if at least one of them is an interferometer, the angle between its arms is equal to $\pi/2$ (L-shaped geometry). In this situation, by definition, $\gamma(f) = 1$. When the detectors are shifted apart (so there is a phase shift between the signals in the two detectors), or rotated out of coalignment (so the detectors have different sensitivity to the same polarization) it turns out that: $|\gamma(f)| < 1$.

The pattern functions (or orientation factors) of a GW detector can be written in the following form

$$F^A(\hat{r},\hat{\Omega},\psi) = \mathrm{Tr}\,\{D(\hat{r})\,\varepsilon^A(\hat{\Omega},\psi)\} \tag{B.7}$$

where the symmetric, trace-less tensor $D(\hat{r})$ describes the orientation and geometry of the detector located at $\vec{r}$.

The tensor $D(\hat{r})$ depends upon the geometrical features of the detector. For instance, in the case of an interferometer, indicating with $\hat{u}$ and $\hat{v}$ the unit vectors in the directions of its arms, one has:

$$D(\hat{r}) = \frac{1}{2}\left\{\hat{u}(\hat{r})\otimes\hat{u}(\hat{r}) \;-\; \hat{v}(\hat{r})\otimes\hat{v}(\hat{r})\right\}. \tag{B.8}$$

In the case of the lowest longitudinal mode of a cylindrical GW antenna with axis in the direction determined by the unit vector $\hat{l}$, one has

$$D(\hat{r}) = \hat{l}(\hat{r})\otimes\hat{l}(\hat{r}) \;-\; \frac{1}{3}I\,, \tag{B.9}$$

where I is the unit matrix. Finally, in the case of the lowest five degenerate quadrupole modes ($m = -2, \ldots, +2$) of a spherical detector, the corresponding tensors are

$$
\begin{aligned}
D^{\,(0)}\,(\hat{r}) &= \frac{1}{2\sqrt{3}}\left\{e^{+}(\hat{r}) \,+\, 2\,g^{+}(\hat{r})\right\} \,=\, \frac{1}{2\sqrt{3}}\left\{2\,f^{+}(\hat{r}) \,-\, e^{+}(\hat{r})\right\} \\
D^{\,(+1)}\,(\hat{r}) &= -\frac{1}{2}\,g^{\times}(\hat{r}) \qquad\qquad D^{\,(-1)}\,(\hat{r}) = -\frac{1}{2}\,f^{\times}(\hat{r}) \\
D^{\,(+2)}\,(\hat{r}) &= \frac{1}{2}\,e^{+}(\hat{r}) \qquad\qquad D^{\,(-2)}\,(\hat{r}) = -\frac{1}{2}\,e^{\times}(\hat{r})
\end{aligned}
\tag{B.10}
$$

where

$$
\begin{aligned}
f^{+}(\hat{r}) &= \hat{m}(\hat{r}) \otimes \hat{m}(\hat{r}) \,-\, \hat{r} \otimes \hat{r} \qquad\qquad f^{\times}(\hat{r}) = \hat{m}(\hat{r}) \otimes \hat{r} \,+\, \hat{r} \otimes \hat{m}(\hat{r}) \\
g^{+}(\hat{r}) &= \hat{n}(\hat{r}) \otimes \hat{n}(\hat{r}) \,-\, \hat{r} \otimes \hat{r} \qquad\qquad g^{\times}(\hat{r}) = \hat{n}(\hat{r}) \otimes \hat{r} \,+\, \hat{r} \otimes \hat{n}(\hat{r})\,,
\end{aligned}
$$

and $e^{+,\times}(\hat{r})$ are the tensors of Eq. (B.3) written in terms of the unit vectors $\hat{m}(\hat{r})$ and $\hat{n}(\hat{r})$ lying on the plane perpendicular to $\hat{r}$. From these expressions for the tensors D^{ij} and interpreting each of the five modes of a sphere as a single detector, it is possible to show that in the case of coincident detectors one has:

$$
< F_1^A(\hat{r}, \hat{\Omega}, \psi) F_2^B(\hat{r}, \hat{\Omega}, \psi) >_{\hat{\Omega},\psi} = \, c_{12}\, \delta^{AB} \qquad\qquad (A, B = +, \times) \tag{B.11}
$$

where c_{12} depends only on the geometry and the relative orientations of the two detectors. The corresponding values of F (see Eq. (B.6)) for the three different geometries considered (interferometer, cylindrical bar, sphere) are summarized in Table I. By introducing the following notation

$$
\Delta\vec{r} = d\,\hat{s} \qquad\qquad \delta = 2\,\pi\,f\,d\,,
$$

where $\hat{s}$ is the unit vector along the direction connecting the two detectors and d is the distance between them, it can be shown [13] that the overlap reduction function assumes the following form ($D_k = D(\hat{r}_k)$):

$$
\gamma(f) = \rho_0(\delta)\, D_1^{ij}\, D_{2\,ij} \,+\, \rho_1(\delta)\, D_1^{ij}\, D_{2\,i}^{k}\, s_j\, s_k \,+\, \rho_2(\eta)\, D_1^{ij}\, D_2^{kl}\, s_i\, s_j\, s_k\, s_l \tag{B.12}
$$

where

$$
\begin{bmatrix} \rho_0 \\ \rho_1 \\ \rho_2 \end{bmatrix}(\delta) = \frac{1}{F\delta^2} \begin{bmatrix} 2\delta^2 & -4\delta & 2 \\ -4\delta^2 & 16\delta & -20 \\ \delta^2 & -10\delta & 35 \end{bmatrix} \begin{bmatrix} j_0 \\ j_1 \\ j_2 \end{bmatrix}(\delta)\,, \tag{B.13}
$$

with $j_k(\delta)$ the standard spherical Bessel functions:

$$
j_0(\delta) = \frac{\sin\delta}{\delta}\,, \qquad j_1(\delta) = \frac{j_0(\delta) - \cos\delta}{\delta}\,, \qquad j_2(\delta) = 3\,\frac{j_1(\delta)}{\delta} \,-\, j_0(\delta)\,.
$$

TABLE I. The normalization factor F for three different geometries of the detectors: interferometer (ITF), cylindrical bar (BAR), and sphere (SPH). A $\star$ denotes entries that can be obtained from the symmetry of the table.

		ITF	BAR	SPH		
				$m = 0$	$m = \pm 1$	$m = \pm 2$
ITF		2/5	$\star$	$\star$	$\star$	$\star$
BAR		2/5	8/15	$\star$	$\star$	$\star$
SPH	$m = 0$	0	$2\sqrt{3}/15$	2/5	$\star$	$\star$
	$m = \pm 1$	0	0	0	2/5	$\star$
	$m = \pm 2$	2/5	2/5	0	0	2/5

APPENDIX B: BBN BOUNDS

In the case of minimal models the integrals determining the analytical expression of the BBN bound are given by:

$$\mathcal{I}_d = z_s^{-2\beta} \left\{ \frac{1}{54}\,(z_s^2 + 6\,z_s + 18) \,-\, \frac{1}{108}\,\left(\frac{f_{\rm ns}}{f_s}\right)^3 \,\big[\, 2\,(z_s^2 + 6\,z_s + 18) \right.$$
$$\left. - 6\,z_s\,(z_s+6)\,\ln\frac{f_{\rm ns}}{f_s} \,+\, 9\,z_s^2\,\ln^2\frac{f_{ns}}{f_s}\,\big]\right\}\,,$$

$$\mathcal{I}_s = \frac{3}{2\,\beta\,(3-2\beta)} \,+\, \frac{z_s^{2\beta-6}}{2\beta-6} \,-\, \frac{z_s^{-2\beta}}{2\beta}\,. \tag{B.1}$$

In the case of non-minimal models the integrals determining the BBN bound are given by

$$\mathcal{I}_1 = A(\sigma, z_s) \,+\, B(\sigma, z_s)\,\ln z_s \,+\, C(\sigma, z_s)\,\ln^2 z_s\,,$$

$$\mathcal{I}_2 = \frac{z_s^{-4}}{4}\,\left(\, z_s^{\sigma-2} \,+\, z_s^{2+\sigma}\,\right)\,\left(\, z_s^{-4} \,-\, z_r^{-4}\,\right)\,(1 \,+\, \ln z_s)^2\,, \tag{B.2}$$

where and $z_r \,=\, f_1/f_r$ and

$$A(\sigma, z_s) = -\frac{z_s^{2\sigma}}{16\,(\sigma^2-4)^3}\,\left\{\, 13\,z_s^{-2(2+\sigma)}\,(\sigma^2-4)^3 \,-\, 4\,z_s^{-4}\,(\sigma+2)^3\,(2\sigma^2-10\sigma+13)\right.$$
$$\left. + 4\,z_s^{-4(1+\sigma)}\,(\sigma-2)^3\,(2\sigma^2+10\sigma+13) \,-\, z_s^{-2\sigma}\,(13\sigma^6 - 172\sigma^4 + 832\sigma^2 - 1664)\,\right\}\,,$$

$$B(\sigma, z_s) = \frac{z_s^{2\sigma-4}}{4\,(\sigma^2-4)^2}\,\left\{\, 2\,(\sigma+2)^2\,(2\sigma-5) \,-\, 2\,z_s^{-4\sigma}\,(\sigma-2)^2\,(2\sigma+5) \,-\, 5\,z_s^{2\sigma}\,(\sigma^2-4)^2\,\right\}\,, \tag{B.3}$$

$$C(\sigma, z_s) = \frac{z_s^{4-2\sigma}}{2\,(\sigma^2-4)}\,\left\{\, 2 \,-\, z_s^{-4\sigma}\,(\sigma-2) \,+\, \sigma\,z_s^{-2\sigma}\,(\sigma^2-4)\right\}\,.$$

[1] L. P. Grishchuk, Zh. Éksp. Teor. Fiz. **67**, 825 (1974) [Sov. Phys. JETP **40**, 409 (1975)]; L. P. Grishchuk, Usp. Fiz. Nauk. **156**, 297 (1988) [Sov. Phys. Usp. **31**, 940 (1988)];
[2] M. White, D. Scott, and J. Silk, Ann. Rev. Astron. Astrophys **32**, 319 (1994).
[3] L. P. Grishchuk, Usp. Fiz. Nauk. **156**, 297 (1988) [Sov. Phys. Usp. **31**, 940 (1988)].
[4] M. Gasperini and M. Giovannini, Phys. Lett. B **282**, 36 (1992).
[5] D. Babusci and M. Giovannini, Phys. Rev. D **60**, 083511 (1999).
[6] L. P. Grishchuk and M. Solokhin, Phys. Rev. D **43**, 2566 (1991); V. Sahni, Phys. Rev. D **42**, 453 (1990); B. Allen, Phys. Rev. D **37**, 2078 (1988).
[7] K. S. Thorne, in *300 Years of Gravitation*, edited by S. W.Hawking and W. Israel (Cambridge University Press, Cambridge, England, 1987); L. P. Grishchuk, talk given at *34th Rencontres de Moriond: Gravitational Waves and Experimental Gravity*, Les Arcs, France, 23-30 Jan 1999; B. Allen, in Proceedings of the Les Houches School on Astrophysical Sources of Gravitational Waves, edited by J. Marck and J. P. Lasota (Cambridge University Press, Cambridge England, 1996).
[8] L. P. Grishchuk, talk given at *34th Rencontres de Moriond: Gravitational Waves and Experimental Gravity*, Les Arcs, France, 23-30 Jan 1999, gr-qc/9903079.
[9] M. Giovannini, Phys. Rev. D **58**, 083504 (1998); Class. Quant. Grav. **16**, 2905 (1999); Phys. Rev. D (to be published), astro-ph/9903004.
[10] G. Veneziano, Phys. Lett. B **265**, 287 (1991); M. Gasperini, in Proc. of the Second SIGRAV School on *Gravitational Waves in Astrophysics Cosmology and String Theory*, hep-th/9907067.
[11] M. Gasperini and M. Giovannini, Phys. Rev. D **47**, 1519 (1993); R. Brustein, M. Gasperini, M. Giovannini, and G. Veneziano, Phys. Lett. B **361**, 45 (1995); M. Giovannini, Phys. Rev. D **55**, 595 (1997); R. Brustein, M. Gasperini, and G. Veneziano, Phys. Rev. D **55**, 3882 (1997).
[12] P. Michelson, Mon. Not. Roy. Astron. Soc. **227**, 933 (1987).
[13] N. Christensen, Phys. Rev. D **46**, 5250 (1992); E. Flanagan, Phys. Rev. D **48**, 2389 (1993).
[14] B. Allen and J. D. Romano, Phys. Rev. D **59**, 102001 (1999)
[15] K. Danzmann, in *Gravitational Wave Experiments*, edited by E. Coccia, G. Pizzella, F. Ronga (World Scientific, Singapore, 1995).
[16] F. J. Raab, in *Gravitational Wave Experiments*, edited by E. Coccia, G. Pizzella, F. Ronga (World Scientific, Singapore, 1995).
[17] K. Tsubono, in *Gravitational Wave Experiments*, edited by E. Coccia, G. Pizzella, F. Ronga (World Scientific, Singapore, 1995).
[18] B. Caron et al., Class. Quantum Grav. **14**, 1461 (1997).
[19] **The importance of building an advanced high-tech interferometer in Europe has been clearly stated during the** *European Gravitational Wave Meeting***, held in London on 27 May 1999 (A. Giazotto, private communication).**
[20] D. Babusci and M. Giovannini, in preparation.
[21] E. Cuoco, G. Curci, and M. Beccaria, to appear in the Proceedings of the 2nd Edoardo Amaldi Conference, Geneva, Switzerland, 1997, gr-qc/9709041.
[22] V. F. Schwartzman, Pis'ma Zh. Éksp. Teor. Fiz **9**, 315 (1969) [JETP Lett **9**, 184 (1969)].
[23] T. Walker et al., Astrophys. J. **376**, 51 (1991).
[24] C. Copi et al., Phys. Rev. Lett. **75**, 3981 (1995); R. E. Lopez and M. S. Turner, Phys. Rev. D **59**, 103502 (1999).
[25] C. L. Bennett, A. Banday, K. M. Gorski, G. Hinshaw, P. Jackson, P. Keegstra, A. Kogut, G. F. Smoot, D. T. Wilkinson, and E. L. Wright, Astrophys. J. **464**, L1 (1996).
[26] V. Kaspi, J. Taylor, and M. Ryba, Astrophy. J. **428**, 713 (1994).
[27] V. A. Rubakov, M. V. Sazhin, and A. V. Veryaskin, Phys. Lett. B **115**, 189 (1982); R. Fabbri and M. D. Pollock, Phys. Lett. B **125**, 445 (1983); L. F. Abbott and M. B. Wise, Nucl. Phys. **224**, 541 (1984).
[28] T. Vachaspati and A. Vilenkin, Phys. Rev. D **31**, 3052 (1985).
[29] M. Giovannini, Phys. Rev. D **58**, 124027 (1998); Phys. Rev. D (to be published), hep-ph/9905358; Phys. Rev. D (to be published), hep-ph/9906241.
[30] M. Giovannini and M. Shaposhnikov, Phys. Rev. D **57**, 2186 (1998); Phys. Rev. Lett. **80**, 22 (1998).
[31] M. Gasperini, in *String theory in curved space times*, Paris 1996, p. 333
[32] V. Kaplunovsky, Phys. Rev. Lett. **55**, 1036 (1985).
[33] P. R. Saulson, *Fundamentals of interferometric gravitational wave detectors*, (World Scientific, 1994).